



Correction to: A Single-Molecule Magnet Tetranuclear $[\text{Mn}^{\text{III}}\text{Mn}^{\text{IV}}\text{O}_3\text{Cl}]$ Complex with Bis(diisopropylphosphinyl)imide Ligands

Wai-Man Cheung¹ · Qian-Feng Zhang² · Rodolphe Clérac^{3,4} · Ian J. Hewitt⁵ · Christopher E. Anson⁵ · Annie K. Powell^{5,6} · Wolfgang Wernsdorfer^{7,6} · Ian D. Williams¹ · Wa-Hung Leung¹

Published online: 29 October 2019

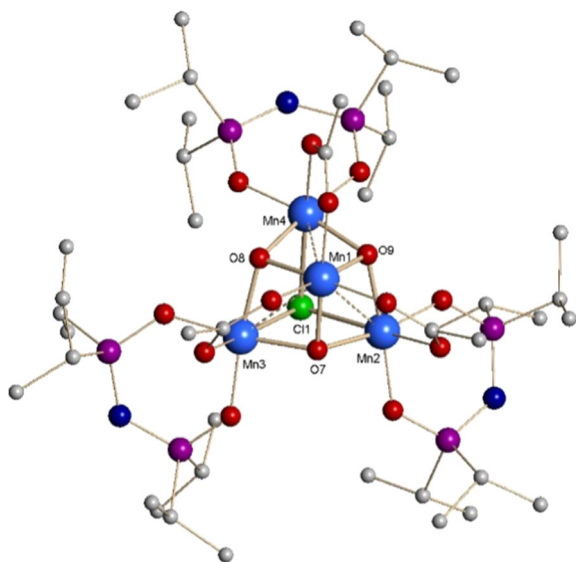
© Springer Science+Business Media, LLC, part of Springer Nature 2019

Abstract

Treatment of $\text{Mn}(\text{OAc})_2 \cdot 4\text{H}_2\text{O}$ with 3 equiv. $\text{HN}(\text{iPr}_2\text{PO})_2$ in the presence of ${}^n\text{Bu}_4\text{NCl}$ in acetonitrile resulted in isolation of a tetranuclear $\{\text{Mn}^{\text{III}}\text{Mn}^{\text{IV}}\}$ complex $[\text{Mn}_4(\mu_3\text{-O})_3(\mu_3\text{-Cl})(\mu\text{-OAc})_3\{\text{N}(\text{iPr}_2\text{PO})_2\}_3] \cdot 0.5\text{C}_6\text{H}_{14}$ (**1**·0.5 C_6H_{14}), and a dinuclear $\{\text{Mn}^{\text{II}}\text{Mn}^{\text{III}}\}$ complex $[\text{Mn}_2\{\text{N}(\text{iPr}_2\text{PO})_2\}_2\{\mu_2, \eta^3\text{-}(\text{iPr}_2\text{PO})_2\text{NH}(\text{iPr}_2\text{PO})\}_2\{\eta^2\text{-}(\text{iPr}_2\text{PO})_2\text{NH}(\text{iPr}_2\text{PO})\}_2] \cdot 0.25\text{AcOH}$ (**2**·0.25AcOH) with bis(diisopropylphosphinyl)imide ligands. The solid-state structures of two complexes have been established by single-crystal X-ray crystallography. The tetranuclear complex **1** belongs to a family of $\{\text{Mn}_3^{\text{III}}\text{Mn}^{\text{IV}}\text{O}_3\text{X}\}$ single-molecule magnets (SMMs) with effective energy barrier of 14.3 K by some further magnetic characterizations.

Graphic Abstract

A $[\text{Mn}_3^{\text{III}}\text{Mn}^{\text{IV}}\text{O}_3\text{Cl}]$ -core-based $[\text{Mn}_4(\mu_3\text{-O})_3(\mu_3\text{-Cl})(\text{OAc})_3\{\text{N}(\text{iPr}_2\text{PO})_2\}_3]$ complex with single-molecule magnet (SMM) behaviour was prepared and structurally characterized, exhibiting slow magnetization relaxation under zero applied dc field with $\tau_0 = 9.0 \times 10^{-7}$ s and relaxation barrier $U_{\text{eff}} = 14.3$ K.



The original article can be found online at <https://doi.org/10.1007/s10876-018-1442-y>.

The original version of this article unfortunately published with wrong author group. It also had several mistakes in text. The author group and errors are corrected in this erratum article.

✉ Qian-Feng Zhang
zhangqf@ahut.edu.cn

✉ Annie K. Powell
annie.powell@kit.edu

✉ Wa-Hung Leung
chleung@ust.hk

Keywords Manganese · Single molecule magnet (SMM) · Mixed-valence manganese complex · Bis(diisopropylphosphinyl)imide ligand · Crystal structure

Introduction

As the smallest known units with the ability of storing up to one bit of information per molecule at cryogenic temperatures, single-molecule magnets (SMMs) have attracted intense research activity in past decades [1–6]. Synthetic chemists have been able to synthesize various polynuclear manganese complexes, such as the dodecanuclear complexes $[\text{Mn}_{12}\text{O}_{12}(\text{O}_2\text{CR})_{16}(\text{H}_2\text{O})_x]$ ($\text{R} = \text{Me}, \text{Et}, \text{Ph}; x = 3, 4$) [7, 8], the polyoxometalate-based $\{\text{Mn}_2^{\text{IV}}\text{Mn}_6^{\text{III}}\text{Mn}_4^{\text{II}}\}$ complexes [9], a family of cationic oxime-based Mn_6^{III} complexes [10], and the high nuclearity mixed-valence $\{\text{Mn}_{32}\}$ complex [11], which show SMM features at the very lowest temperatures, but examples of homometallic Mn-based SMMS with blocking temperatures above 1 K are still relatively unusual. Among them is a family of tetranuclear mixed-valence manganese complexes with general formula $[\text{Mn}_4\text{O}_3\text{X}(\text{OAc})_3(\text{dbm})_3]$ and the core $[\text{Mn}_4(\mu_3\text{-O})_3(\mu_3\text{-X})]^{6+}$, where $\text{X} = \text{Br}^-, \text{Cl}^-, \text{OAc}^-$ and F^- , OAc^- is the acetate ion and dbm^- is the anion of dibenzoylmethane [12]. These $\{\text{Mn}_3^{\text{III}}\text{Mn}^{\text{IV}}\}$ complexes possess a well-isolated ground-state spin of $S = 9/2$, displaying hysteresis loops containing Quantum Tunnelling of the Magnetization (QTM) steps and exhibiting SMM behavior with an energy barrier of the order of 14.5 K [13]. On the other hand, stronger electron-donating phosphinate and phosphonate derivatives could stabilize the mixed-valence $\{\text{Mn}^{\text{III}}\text{Mn}^{\text{II}}\}$ complexes with large spin and coercivity [14–16]. With this in mind, we report synthesis, structure and magnetic properties of a tetranuclear

$\{\text{Mn}_3^{\text{III}}\text{Mn}^{\text{IV}}\}$ complex with bis(diisopropylphosphinyl)imide ligands, $[\text{Mn}_4(\mu_3\text{-O})_3(\mu_3\text{-Cl})(\text{OAc})_3\{\text{N}(\text{iPr}_2\text{PO})_2\}_3]$ (**1**), which belongs to the above-mentioned $\{\text{Mn}_4\text{O}_3\text{X}\}$ family. Results of magnetic measurements show that the tetranuclear complex **1** exhibits SMM behavior.

Experimental

Materials and Measurements

All the reagents were commercially purchased and used without further purification. The $\text{HN}(\text{iPr}_2\text{PO})_2$ ligand was synthesized according to the literature [17]. Elemental analyses were carried out using a Perkin-Elmer 2400 CHN analyzer.

Synthesis of $[\text{Mn}_4(\mu_3\text{-O})_3(\mu_3\text{-Cl})(\mu\text{-OAc})_3\{\text{N}(\text{iPr}_2\text{PO})_2\}_3] \cdot 0.5\text{C}_6\text{H}_{14}$ (**1**·0.5C₆H₁₄) and $[\text{Mn}_2\{\text{N}(\text{iPr}_2\text{PO})_2\}\{\mu_2,\eta^3\text{-}(\text{iPrPO}_2)\text{NH}(\text{iPr}_2\text{PO})\}_2\{\eta^2\text{-}(\text{iPrPO}_2)\text{NH}(\text{iPr}_2\text{PO})\}_2] \cdot 0.25\text{AcOH}$ (**2**·0.25AcOH)

To a suspension of $\text{Mn}(\text{OAc})_2 \cdot 4\text{H}_2\text{O}$ (95 mg, 1.0 mmol) in acetonitrile (10 mL) was added $\text{HN}(\text{iPr}_2\text{PO})_2$ (84 mg, 3.0 mmol) and $n\text{-Bu}_4\text{NCl}$ (70 mg, 0.25 mmol) in the air. The reaction mixture was stirred overnight at room temperature. The volatile was removed by rotation evaporation. The brown residue was extracted with hexane and then filtered. Evaporation of the hexane solution afforded complex **1**·0.5C₆H₁₄ as red plate-shaped crystals and complex **2**·0.25AcOH as pink prism-shaped crystals, both suitable for crystallography. Note that yields have not been optimized. Two complexes may be separated by a physical method in light of their different colors and shapes of crystalline products. Yield of **1**·0.5C₆H₁₄: 20 mg, 6% (based on Mn). Anal. Calcd. for $\text{C}_{45}\text{H}_{100}\text{O}_{15}\text{N}_3\text{ClP}_6\text{Mn}_4$: C, 39.62; H, 7.39; N, 3.08%. Found: C, 39.66; H, 7.42; N, 3.12%. Yield of **2**·0.25AcOH: 28 mg, 4% (based on Mn). Anal. Calcd. for $\text{C}_{48.50}\text{H}_{117}\text{O}_{14.50}\text{N}_5\text{P}_{10}\text{Mn}_2$: C, 40.96; H, 8.29; N, 4.92%. Found: C, 40.93; H, 8.26; N, 4.90%.

Crystal Structure Determinations

A summary of crystallographic data and experimental details for complexes **1**·0.5C₆H₁₄ and **2**·0.25AcOH are listed in Table 1. Intensity data were collected on a Bruker

- Department of Chemistry, The Hong Kong University of Science and Technology, Clear Water Bay, Kowloon, Hong Kong, People's Republic of China
- Institute of Molecular Engineering and Applied Chemistry, Anhui University of Technology, Ma'anshan 243002, Anhui, People's Republic of China
- CNRS, CRPP, UMR 5031, 33600 Pessac, France
- University of Bordeaux, CRPP, UMR 5031, 3360 Pessac, France
- Institut für Anorganische Chemie, Karlsruhe Institute of Technology, Engesserstrasse 15, 76131 Karlsruhe, Germany
- Institute of Nanotechnology, Karlsruhe Institute of Technology, Hermann-von-Helmholtz-Platz 1, 76344 Eggenstein-Leopoldshafen, Germany
- Physikalisches Institut, Karlsruhe Institute of Technology, Wolfgang-Gaede-Str. 1, 76131 Karlsruhe, Germany

Table 1 Crystallographic data and experimental details for [Mn₄(μ₃-O)₃(μ₃-Cl)-(μ-OAc)₃{N(ⁱPr₂PO)₂}₃].0.5C₆H₁₄ (**1**·0.5C₆H₁₄), and [Mn₂{N(ⁱPr₂PO)₂}₂]{μ₂-η³-(ⁱPrPO₂)NH(ⁱPr₂PO)}₂{η²-(ⁱPrPO₂)NH(ⁱPr₂PO)}₂].0.25AcOH (**2**·0.25AcOH)

Complex	1 ·0.5C ₆ H ₁₄	2 ·0.25CH ₃ CO ₂ H
Empirical formula	C ₄₅ H ₁₀₀ ClMn ₄ N ₃ O ₁₅ P ₆	C _{48.50} H ₁₁₇ Mn ₂ N ₅ O _{14.50} P ₁₀
Formula weight	1364.31	1422.04
Crystal system	triclinic	triclinic
Space group	<i>P</i> $\bar{1}$	<i>P</i> $\bar{1}$
<i>a</i> (Å)	12.1543 (15)	13.4952 (13)
<i>b</i> (Å)	20.683 (2)	14.5487 (14)
<i>c</i> (Å)	27.320 (3)	20.661 (2)
α (°)	107.965 (2)	110.344 (2)
β (°)	92.601 (2)	98.465 (2)
γ (°)	95.963 (2)	102.756 (2)
<i>V</i> (Å ³)	6476.0 (13)	3596.6 (6)
<i>Z</i>	4	2
<i>D</i> _{calcd} (g cm ⁻³)	1.399	1.313
Temperature (K)	100 (2)	100 (2)
<i>F</i> (000) (<i>e</i>)	2872	1518
μ (Mo-K α) (mm ⁻¹)	1.010	0.631
Refl. total	34,280	19,299
Refl. unique/ <i>R</i> _{int}	22,366/0.0707	12,399/0.0594
Ref. parameters	1333	724
<i>R</i> 1 ^a , <i>wR</i> 2 ^b [<i>I</i> > 2 σ (<i>I</i>)]	0.0592, 0.0962	0.0600, 0.1174
<i>R</i> 1 ^a , <i>wR</i> 2 ^b (all data)	0.1449, 0.1121	0.1215, 0.1345
GoF ^c	1.012	0.880
$\Delta\rho_{\text{fin}}$ (max/min) (<i>e</i> Å ⁻³)	+ 0.703/− 0.548	+ 0.966/− 0.459

$$^a R1 = \sum ||F_o| - |F_c|| / \sum |F_o|$$

$$^b wR2 = [\sum w(F_o^2 - F_c^2)^2 / \sum w(F_o^2)]^{1/2}, w = [\sigma^2(F_o^2) + (AP)^2 + BP]^{-1}, \text{ where } P = (\text{Max}(F_o^2, 0) + 2F_c^2) / 3$$

$$^c \text{GoF} = S = [\sum w(F_o^2 - F_c^2)^2 / (n_{\text{obs}} - n_{\text{param}})]^{1/2}$$

SMART APEX 2000 CCD diffractometer using graphite-monochromated Mo-K α radiation ($\lambda = 0.71073$ Å) at 100(2) K. The data were corrected for absorption using the program SADABS [18]. Structures were solved by the direct methods and refined by full-matrix least-squares on *F*² using the SHELXTL software package [19, 20]. All non-hydrogen atoms were refined anisotropically except for the solvent molecules due to disorder. Hydrogen atoms in the phenyl and other organic moieties were treated as idealized contributions (C_{sp3}-H = 0.96, C_{sp2}-H = 0.93 Å, and N-H 0.86 Å). CCDC reference numbers 1844319 and 1844320 contain the supplementary crystallographic data for this paper. Copies of the data can be obtained free of charge on application to CCDC, 12 Union Road, Cambridge CB2 1EZ, UK [fax: (+44)1233-336-033; e-mail: deposit@ccdc.cam.ac.uk].

Magnetic Measurements

Magnetic data (ac and dc) were recorded on a Quantum Design MPMS-XL SQUID magnetometer equipped with a 7 T magnet and capable of operating in the 1.8–300 K temperature range. Ac magnetic susceptibility measurements were performed in an oscillating ac field of 3.5 G and a zero dc field. The oscillation frequencies were in the 10–1000 Hz range. Diamagnetic corrections to the observed susceptibilities were applied using Pascal's constant.

Magnetic studies below 1.8 K were carried out on the single-crystals using a micro-SQUID apparatus operating down to 0.04 K [21]. The samples were cooled at 10 K/min under 1 atm of helium gas. Temperature control was achieved within the variable-flow cryostat belonging to a Quantum Design PPMS system. A well-formed plate-like crystal was indexed, and mounted with the applied magnetic field normal to the dominant (010) face. The two independent cluster molecules have their respective

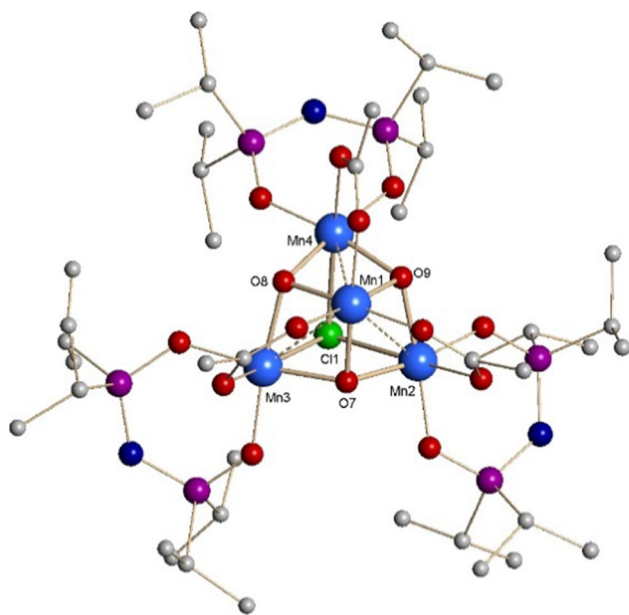


Fig. 1 Structure of one of the two Mn_4 molecules in $1 \cdot 0.5\text{C}_6\text{H}_{14}$. Selected bond lengths (Å) and angles (deg): Mn1...Mn2, 2.8053(12); Mn1...Mn3, 2.8003(13); Mn1...Mn4, 2.8023(13); Mn2...Mn3, 3.2160(12); Mn3...Mn4, 3.2734(12); Mn2...Mn4, 3.2344(12); Mn2–Cl1, 2.6256(17); Mn3–Cl1, 2.6130(17); Mn4–Cl1, 2.6434(17); O7–Mn(1,2,3), 1.846(4), 1.920(4), 1.931(4), respectively; O8–Mn(1,3,4), 1.847(4), 1.936(4), 1.959(4), respectively; O9–Mn(1,2,4), 1.853(4), 1.941(4), 1.916(4), respectively; Mn2–Cl1–Mn3, 75.75(5); Mn2–Cl1–Mn4, 75.74(5); Mn3–Cl1–Mn4, 77.03(5); Mn1–O7–Mn2, 96.29(16); Mn1–O7–Mn3, 95.68(15); Mn2–O7–Mn3, 113.24(19); Mn1–O8–Mn3, 95.48(15); Mn1–O8–Mn4, 94.78(15); Mn3–O8–Mn4, 114.37(18); Mn1–O9–Mn2, 95.31(16); Mn1–O9–Mn4, 96.04(15); Mn2–O9–Mn4, 113.97(19)

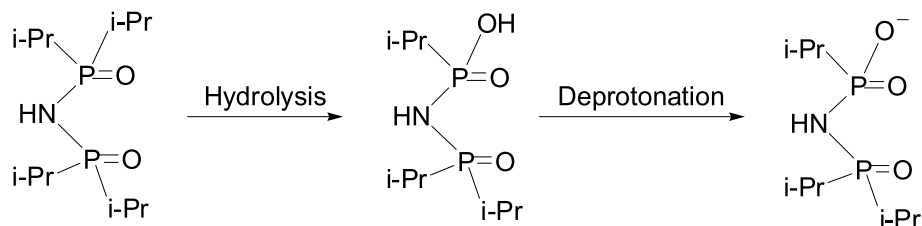
threefold axes close to co-parallel, with both inclined by ca. 45° to the normal to the (010) face. Thus all the molecular threefold axes subtended an angle of ca. 45° to the applied magnetic field.

Results and Discussion

Syntheses and Crystal Structures

Treatment of $\text{Mn}(\text{OAc})_2 \cdot 4\text{H}_2\text{O}$ in acetonitrile with ca. 3 equiv. $\text{HN}(\text{}^i\text{Pr}_2\text{PO})_2$ in the presence of ${}^n\text{Bu}_4\text{NCl}$ resulted in isolation of the tetranuclear $\{\text{Mn}^{\text{III}}\text{Mn}^{\text{IV}}\}$ complex $[\text{Mn}_4(\mu_3\text{-O})_3(\mu_3\text{-Cl})(\mu\text{-OAc})_3\{\text{N}(\text{}^i\text{Pr}_2\text{PO})_2\}_3] \cdot 0.5\text{C}_6\text{H}_{14}$

Fig. 2 Partial hydrolysis of the ligand $\text{HN}(\text{}^i\text{Pr}_2\text{PO})_2$ and its possible deprotonated form



$(1 \cdot 0.5\text{C}_6\text{H}_{14})$ as red crystals and the dinuclear $\{\text{Mn}^{\text{III}}\text{Mn}^{\text{II}}\}$ complex $[\text{Mn}_2\{\text{N}(\text{}^i\text{Pr}_2\text{PO})_2\}\{\mu_2,\eta^3\text{-}(\text{}^i\text{PrPO}_2)\text{NH}(\text{}^i\text{Pr}_2\text{PO})\}_2\{\eta^2\text{-}(\text{}^i\text{PrPO}_2)\text{NH}(\text{}^i\text{Pr}_2\text{PO})\}_2] \cdot 0.25\text{AcOH}$ ($2 \cdot 0.25\text{AcOH}$) as pink crystals in 5–10% non-optimized yields. Complexes $1 \cdot 0.5\text{C}_6\text{H}_{14}$ and $2 \cdot 0.25\text{AcOH}$ may be physically separated according to their obviously different colors and shapes. The previously reported and structurally-similar complex $[\text{Mn}_4\text{O}_3\text{Cl}(\text{OAc})_3(\text{dbm})_3]$ was synthesized by treatment of $[\text{Mn}_4\text{O}_2(\text{OAc})_6(\text{py})_2(\text{dbm})_2]$ with ${}^n\text{Bu}_4\text{NCl}$ or Me_3SiCl in dichloromethane ($\text{py} = \text{pyridine}$) [22]. Single-crystal X-ray diffraction analysis reveals that structure of the tetranuclear $1 \cdot 0.5\text{C}_6\text{H}_{14}$ (red crystals) consists of a distorted cubane core $[\text{Mn}_4(\mu_3\text{-O})_3(\mu_3\text{-Cl})]$ with Mn1 as the Mn^{IV} . Bond valence sum analysis [25, 26] resulted in calculated valences of 4.05 and 4.11 for Mn1A and Mn1B, with the remaining Mn sites all having valences in the range 3.11–3.22 (Fig. 1). The asymmetric unit contains two independent cluster molecules, but these are closely isostructural and that containing Mn1 will be described here. Three AcO^- groups bridge each $\{\text{Mn}^{\text{III}}\text{Mn}^{\text{IV}}\}$ pair, and three chelating $[\text{N}(\text{}^i\text{Pr}_2\text{PO})_2]^-$ ions on each Mn^{III} complete the peripheral ligation. The $\{\text{Mn}_4\text{O}_3\text{Cl}\}$ core of complex $1 \cdot 0.5\text{C}_6\text{H}_{14}$ is essentially superimposable on those of other $\{\text{Mn}_4\text{O}_3\text{Cl}\}$ complexes [13, 22]. For example, the $\text{Mn}^{\text{III}}\cdots\text{Mn}^{\text{III}}$ separations [3.2288(12)–3.2891(12) Å] and $\text{Mn}^{\text{III}}\cdots\text{Mn}^{\text{IV}}$ distances [2.8002(13)–2.8048(12) Å] in complex $1 \cdot 0.5\text{C}_6\text{H}_{14}$ are similar to those in $[\text{Mn}_4\text{O}_3\text{Cl}(\text{OAc})_3(\text{dbm})_3]$ [$\text{Mn}^{\text{III}}\cdots\text{Mn}^{\text{III}} = 3.237(5)\text{--}3.264(4)$ Å, $\text{Mn}^{\text{III}}\cdots\text{Mn}^{\text{IV}} = 2.792(5)\text{--}2.797(4)$ Å] [22], showing that the complete exchange of oxygen-ligating ligands ($[\text{N}(\text{}^i\text{Pr}_2\text{PO})_2]^-$) for the previously present peripheral ligands (py , imidazole, Cl^- , dbm^-) has little structural effect. The $\text{Mn}^{\text{IV}}\text{-O}$ bond lengths of 1.846(4)–1.853(3) Å are a little shorter than those of $\text{Mn}^{\text{III}}\text{-O}$ bond lengths [1.916(4)–1.959(3) Å] in complex $1 \cdot 0.5\text{C}_6\text{H}_{14}$. The P–O lengths [1.531(4)–1.541(4) Å] and P–N lengths [1.582(5)–1.599(5) Å] of the three $[\text{N}(\text{}^i\text{Pr}_2\text{PO})_2]^-$ groups in complex $1 \cdot 0.5\text{C}_6\text{H}_{14}$ indicate a good π -electron delocalized ligand system [23, 24].

The structure of $[\text{Mn}_2\{\text{N}(\text{}^i\text{Pr}_2\text{PO})_2\}\{\mu_2,\eta^3\text{-}(\text{}^i\text{PrPO}_2)\text{NH}(\text{}^i\text{Pr}_2\text{PO})\}_2] \cdot 0.25\text{AcOH}$ ($2 \cdot 0.25\text{AcOH}$) is a dinuclear $\{\text{Mn}^{\text{II}}\text{Mn}^{\text{III}}\}$ complex bridged by two $[\eta^3\text{-}(\text{}^i\text{PrPO}_2)\text{NH}(\text{}^i\text{Pr}_2\text{PO})]^-$ ligands which were probably generated by partial hydrolysis of the

Fig. 3 a Framework of complex $2\cdot 0.25\text{CH}_3\text{CO}_2\text{H}$. Carbons, hydrogens and the acetic acid molecule were omitted. Selected bond lengths (\AA) and angles (deg): Mn1–O(1,2,3,4,5,6), 1.898(3), 2.210(3), 1.901(3), 2.198(3), 1.899(3), 1.908(3), respectively; Mn2–O(7,8,9,10,11,12), 2.177(3), 2.181(3), 2.187(3), 2.160(3), 2.175(3), 2.202(3), respectively; P1–O(1,11), 1.511(3), 1.489(3), respectively; P2–O2, 1.496(3); P3–O(3,12) 1.527(3), 1.475(3), respectively; P4–O4, 1.490(3); P5–O5, 1.535(3); P6–O6, 1.525(3); P7–O(7,13), 1.518(3), 1.485(3), respectively; P8–O8, 1.490(3); P9–O(9,14), 1.507(3), 1.497(3), respectively; P10–O10, 1.495(3); O1–Mn1–O2, 86.57(12); O3–Mn1–O4, 87.11(12); O5–Mn1–O6, 92.33(13); O7–Mn2–O8, 82.62(11); O9–Mn2–O10, 82.51(11). **b** Structure of complex $2\cdot 0.25\text{CH}_3\text{CO}_2\text{H}$. Hydrogens and the acetic acid molecule were omitted

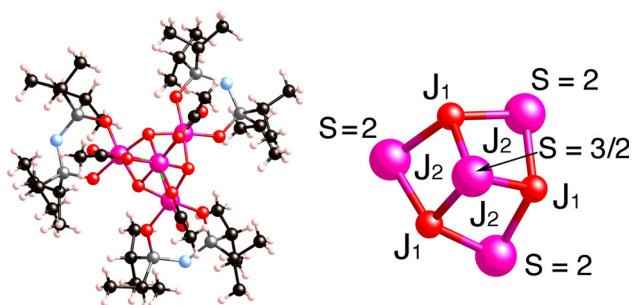
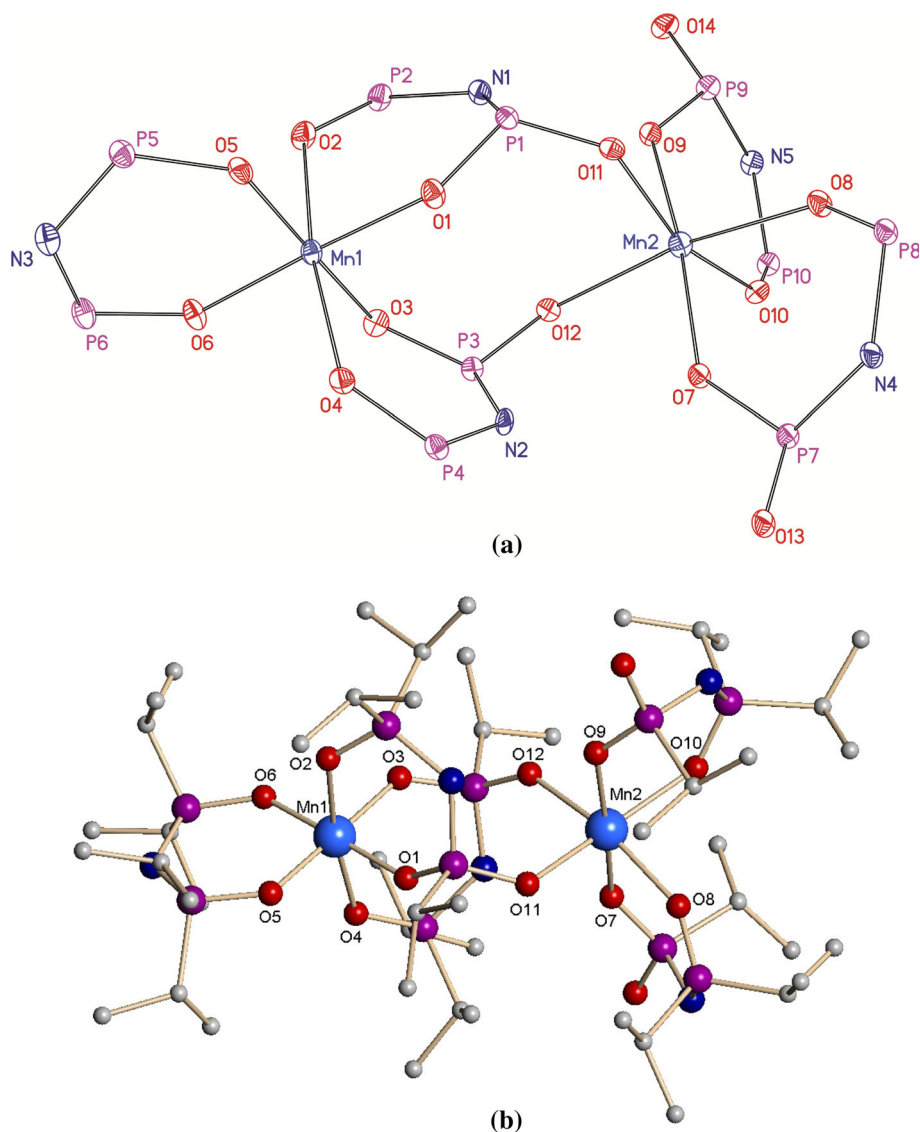


Fig. 4 a The structure of $1\cdot 0.5\text{C}_6\text{H}_{14}$ viewed along the pseudo- C_3 axis. The Mn ions are shown in pink with the Mn^{IV} center. **b** Schematic representation of the exchange coupling in $1\cdot 0.5\text{C}_6\text{H}_{14}$ with the principal exchange pathways J_1 and J_2

$\text{HN}(\text{Pr}_2\text{PO})_2$ ligand in wet solution (Fig. 2). The assignment of the oxidation states for the manganese ions were once again confirmed by bond valence sum calculations.

The valence sums [25, 26] for Mn1 (3.09) and Mn2 (1.95) are in good agreement with the expected valences of +3 and +2. The Mn1 is six-coordinated by two oxygen atoms from the $[\text{N}(\text{Pr}_2\text{PO})_2]^-$ ligand and four oxygen atoms from two bridging $[\eta^3\text{-}(\text{PrPO}_2)\text{NH}(\text{Pr}_2\text{PO})]^-$ ligands, while the Mn2 is six-coordinated to two oxygen atoms from two bridging $[\eta^3\text{-}(\text{PrPO}_2)\text{NH}(\text{Pr}_2\text{PO})]^-$ ligands and four oxygen atoms from two chelating $[\eta^2\text{-}(\text{PrPO}_2)\text{NH}(\text{Pr}_2\text{PO})]^-$ ligands (Fig. 3). The average Mn1–O and Mn2–O lengths in $2\cdot 0.25\text{AcOH}$ are 2.002(3) and 2.180(3) \AA , respectively, which are consistent with the typical bond lengths of $\text{Mn}^{\text{III}}\text{-O}$ and $\text{Mn}^{\text{II}}\text{-O}$, respectively [9]. The N–P bond lengths ranging from 1.649(4) to 1.684(4) \AA in the $[(\text{PrPO}_2)\text{NH}(\text{Pr}_2\text{PO})]^-$ ligands are longer than those in the $[\text{N}(\text{Pr}_2\text{PO})_2]^-$ ligand (1.579(4) and 1.596(4) \AA) in complex $2\cdot 0.25\text{AcOH}$, suggesting characteristic of single bond as

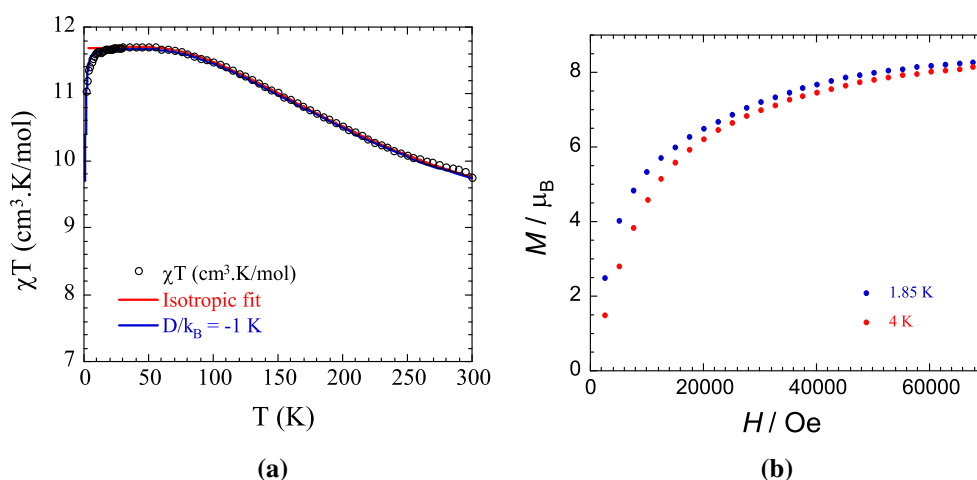


Fig. 5 **a** Plots of χT versus T for complex **1-0.5C₆H₁₄** in an applied field of 1000 Oe in the 2.0–300 K range. **b** Field dependence of the magnetization at 1.85 K and 4 K for complex **1-0.5C₆H₁₄**

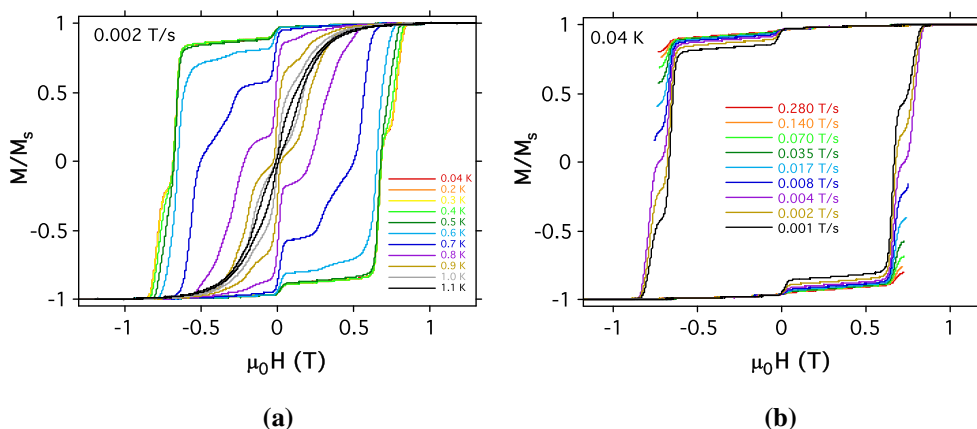


Fig. 6 Magnetization (M) versus dc field hysteresis loops for **1-0.5C₆H₁₄** at the indicated temperatures and a fixed field sweep rate of 0.002 T/s (**a**), and at the indicated field sweep rates and a fixed temperature 0.04 K (**b**) by the micro-SQUID technique with the

magnetic field applied normal to the (010) face and at ca. 45° to the molecular threefold axes. The magnetization is normalized to its saturation value, M_S

shown in Chart 1. The Mn1...Mn₂ separation is ca. 5.327 Å in the non-planar eight-membered ring Mn₂O₄P₂.

Magnetic Properties

Based on the structure of tetranuclear complex **1**, the molecular point symmetry is approximately C_{3v} with the C_3 axis passing through the Mn^{IV} and Cl⁻ ions (Fig. 4). The average angle (α) between the three JT elongation axes and the molecular anisotropy axis (i.e., the virtual C_3 axis) is $\sim 45.4^\circ$ like in [Mn₄O₃Cl(OAc)₃(dbm)₃] (45.1°) [22]. To model the magnetic properties using an isotropic Heisenberg model in the weak field approximation, we simulated the χT product taking into account only two isotropic intra-cluster magnetic interactions between Mn^{III} ($S = 2$) and Mn^{IV} ($S = 3/2$) sites and neglecting the low temperature data (below 20 K) to avoid the influence of the

anisotropy and weak inter-cluster interactions. The following spin-Hamiltonian is considered [22]:

$$H = -2J_1(S_1 \cdot S_2 + S_1 \cdot S_3 + S_2 \cdot S_3) - 2J_2(S_4 \cdot (S_1 + S_2 + S_3))$$

with $S_1 = S_2 = S_3 = 2$ for the Mn^{III} ions and $S_4 = 3/2$ for the Mn^{IV} ion, respectively. J_1 and J_2 are the Mn(III)-Mn(III) and Mn(III)-Mn(IV) exchange coupling constants, respectively. The fitting procedure using the deduced susceptibility gave $J_1/k_B = 13.5(2)$ K, $J_2/k_B = -53.1(2)$ K and $g = 1.94$, the magnitude of the magnetic interactions are significantly higher than that in the related complex [Mn₄O₃Cl(OAc)₃(dbm)₃] (11.9 K (8.3 cm^{-1}), -40.8 K (-28.4 cm^{-1}), 1.98) [22]. The value of χT for complex **1-0.5C₆H₁₄** increases from $9.86 \text{ cm}^3 \text{ mol}^{-1} \text{ K}$ at 300 K to a maximum of $11.72 \text{ cm}^3 \text{ mol}^{-1} \text{ K}$ at 25 K and then decreases rapidly to $11.00 \text{ cm}^3 \text{ mol}^{-1} \text{ K}$ at 2.0 K (Fig. 5a).

Fig. 7 Ac susceptibility of complex $1\cdot 0.5\text{C}_6\text{H}_{14}$ in a 3.5 G field oscillating at 10, 100, 500, and 1000 Hz: in-phase signal (χ') and out-of-phase signal (χ'') versus T

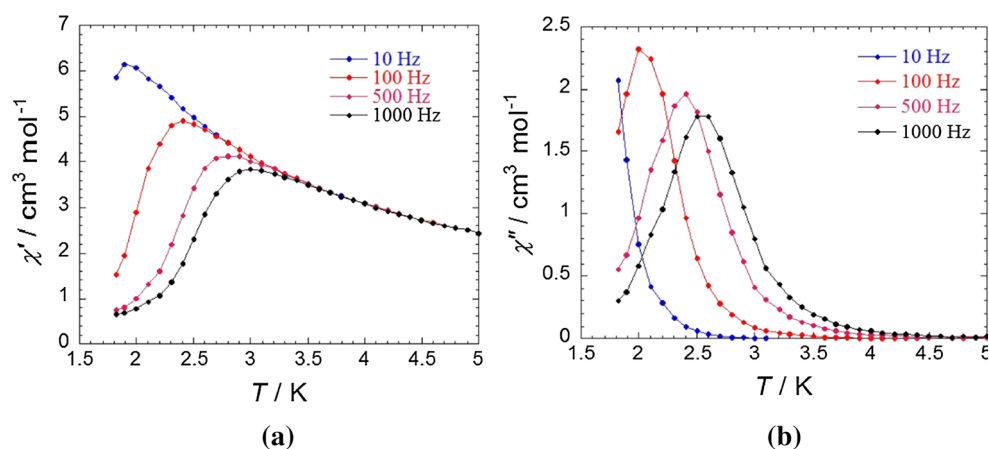
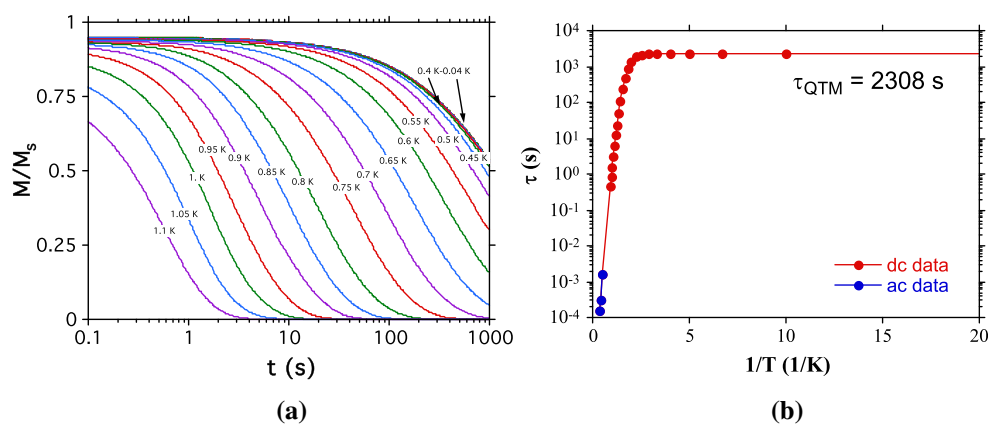


Fig. 8 **a** Relaxation of the magnetization below 1.1 K normalized to the initial magnetization at 0.04 K by the micro-SQUID technique with the magnetic field applied normal to the (010) face and at ca. 45° to the molecular threefold axes. **b** Relaxation time τ versus T^{-1} plot in zero ac and dc field



The maximum χT for $1\cdot 0.5\text{C}_6\text{H}_{14}$ is slightly below the spin-only ($g = 2$) value expected for a complex with an $S = 9/2$ ground state ($12.38 \text{ cm}^3 \text{ mol}^{-1} \text{ K}$), and this is consistent with $g < 2.0$, as expected for Mn [27]. The fit of the temperature dependence of the χT product allows the molecular zero-field splitting parameter D to be determined for $1\cdot 0.5\text{C}_6\text{H}_{14}$. The accuracy of this parameter is rather low; we estimated $D = -1.0(4) \text{ K}$. This is comparable to values from other $\text{Mn}_4\text{O}_3\text{X}$ SMMs (typically $D/k_B = -0.7 \text{ K}$) [2, 27]. The simulation with the fitting with $D/k_B = -1 \text{ K}$ is shown in Figure 5a. It is known that a compound with a large negative D value will show a much lower magnetization at a given field than for Brillouin behaviour. As shown in Fig. 5b, the magnetization value at 7 T of $8.30 \mu_B$ for complex $1\cdot 0.5\text{C}_6\text{H}_{14}$ at 1.85 K is less than the expected saturation magnetization value of $9 \mu_B$.

Hysteresis loops are observed below 1.2 K, confirming the negative value for D (easy-axis behavior) (Fig. 6). These data are strongly temperature and sweep-field rate dependent as expected for the SMM. Nevertheless below 0.5 K, the hysteresis loops at a given scan rate become temperature independent as expected for a Quantum Tunneling regime. Taking the data at the lowest temperature

available: 0.04 K, steps are clearly observed indicative a Quantum Tunneling of the Magnetization (QTM, in zero-field). Slow relaxation of the magnetization is also observed by ac susceptibility measurements. Traditional feature of the SMM is observed with strongly frequency dependence in-phase and out-of-phase ac susceptibilities (Fig. 7). Using these data in addition to the direct relaxation of the magnetization, the relaxation time can be deduced. The same shape of M/M_s versus t curves (where M/M_s is the magnetization normalized to its saturation value) was obtained for the whole temperature range (0.04–1.1 K) (Fig. 8a) and therefore the data were scaled into a single master curve [8]. The relaxation time was extracted simply taking the time when M/M_s reaches the value $1/e$. As indicated by the magnetization measurements, a pure QTM regime is observed below 0.4 K, similar to that of 0.3 K for $[\text{Mn}_4]_2$ dimer [2] and 0.6 K for $[\text{Mn}_4\text{O}_3\text{Cl}(\text{OAc})_3(\text{dbm})_3]$ [22], with a characteristic time $\tau_{\text{QTM}} = 2308 \text{ s}$ (Fig. 8b). The effective energy gap of the thermally activated regime (that can also be influenced by QTM) is about 14.3 K and the τ_0 is about $9 \times 10^{-7} \text{ s}$.

In summary, two mixed-valence Mn_2 and Mn_4 complexes with bis(diisopropylphosphinyl)-imide ligands were

synthesized and isolated with the crystalline state. The Mn₄ complex [Mn₄(μ₃-O)₃(μ₃-Cl)(OAc)₃{N(ⁱPr₂PO)₂}₃] presents the typical feature of SMM and its D/k_B value can be estimated at $-1.0(4)K$. Isolation of the tetranuclear mixed-valence Mn₄ complex may provide a new route for assembly of novel mixed-valence manganese complexes based on Mn₄ cores and new type of phosphinyl-surrounded Mn₄ SMM materials.

Acknowledgements This work was supported by the Hong Kong Research Grants Council (project no. 16307216), the University of Bordeaux, the Région Aquitaine, the CNRS, MAGMANet (NMP3-CT-2005-515767) and the Helmholtz foundation POF-STN. Q.-F.Z. thanks Science and Technological Fund of Anhui Province for an Outstanding Youth Award (06046100).

References

1. S. Hill, R. S. Edwards, N. Aliaga-Alcalde, and G. Christou (2003). *Science* **302**, 1015.
2. W. Wernsdorfer, N. Allaga-Alcalde, D. N. Hendrickson, and G. Christou (2002). *Nature* **416**, 406.
3. G. E. Kostakis, A. M. Ako, and A. K. Powell (2010). *Chem. Soc. Rev.* **39**, 2238.
4. C.-I. Yang, Z.-Z. Zhang, and S.-B. Lin (2015). *Coord. Chem. Rev.* **289–290**, 289.
5. J.-L. Liu, Y.-C. Chen, and M.-L. Tong (2018). *Chem. Soc. Rev.* **47**, 2431.
6. M. Ding, G. E. Cutsail III, D. Aravena, M. Amoza, M. Rouzières, P. Dechambenoit, Y. Losovyj, M. Pink, E. Ruiz, R. Clérac, and J. M. Smith (2016). *Chem. Sci.* **7**, 6132.
7. H. J. Epply, H.-L. Tsai, N. de Vries, K. Folting, G. Christou, and D. N. Hendrickson (1995). *J. Am. Chem. Soc.* **117**, 301.
8. A. Caneschi, D. Gatteschi, R. Sessoli, A.-L. Barra, L.-C. Brunel, and M. Guillot (1991). *J. Am. Chem. Soc.* **113**, 5873.
9. Z.-M. Zhang, S. Yao, Y.-G. Li, H.-H. Wu, Y.-H. Wang, M. Rouzières, R. Clérac, Z.-M. Su, and E.-B. Wang (2013). *Chem. Commun.* **49**, 2515.
10. J. Martinez-Lillo, N. Dolan, and E. K. Brechin (2014). *Dalton Trans.* **43**, 4408.
11. S. K. Langley, R. A. Stott, N. F. Chilton, B. Moubaraki, and K. S. Murray (2011). *Chem. Commun.* **47**, 6281.
12. H. Andres, R. Basler, H. U. Güdel, G. Aromi, G. Christou, H. Büttner, and B. Ruffle (2000). *J. Am. Chem. Soc.* **122**, 12469.
13. A. Sieber, G. Chaboussant, R. Bircher, C. Boskovic, H. U. Güdel, G. Christou, and H. Mutka (2004). *Phys. Rev. B* **70**, 172413.
14. J.-Z. Wu, F. D. Angelis, T. G. Carrell, G. P. A. Yap, J. Sheats, R. Car, and G. C. Dismukes (2006). *Inorg. Chem.* **45**, 189.
15. S. Maheswaran, G. Chastanet, S. J. Teat, T. Mallah, R. Sessoli, W. Wernsdorfer, and R. E. P. Winpenny (2005). *Angew. Chem. Int. Ed.* **44**, 5044.
16. O. A. Adebayo, K. A. Abboud, and G. Christou (2017). *Inorg. Chem.* **56**, 11352.
17. A. R. Chakravarty, F. A. Cotton, D. A. Tocher, and J. H. Tocher (1985). *Organometallics* **4**, 8.
18. G. M. Sheldrick *SADABS* (University of Göttingen, Germany, 1996).
19. G. M. Sheldrick *SHELXTL Software Reference Manual (Version 5.1)* (Bruker AXS Inc., Madison, 1997).
20. G. M. Sheldrick (2008). *Acta Crystallogr. A* **64**, 112.
21. W. Wernsdorfer (2001). *Adv. Chem. Phys.* **118**, 99.
22. S. Wang, H.-L. Tsai, E. Libby, K. Folting, W. E. Streib, D. N. Hendrickson, and G. Christou (1996). *Inorg. Chem.* **35**, 7578.
23. G.-C. Wang, H. Y. Sung, I. D. Williams, and W.-H. Leung (2012). *Inorg. Chem.* **51**, 3640.
24. K.-C. Au-Yeung, Y.-M. So, G.-C. Wang, H. H.-Y. Sung, I. D. Williams, and W.-H. Leung (2016). *Dalton Trans.* **45**, 5434.
25. W. Liu and H. H. Thorp (1993). *Inorg. Chem.* **32**, 4102.
26. D. I. Brown and D. Altermatt (1985). *Acta Crystallogr. Sect. B: Struct. Sci.* **41**, 244.
27. N. Aliaga-Alcalde, R. S. Edwards, S. O. Hill, W. Wernsdorfer, K. Folting, and G. Christou (2004). *J. Am. Chem. Soc.* **126**, 12503.

Publisher's Note Springer Nature remains neutral with regard to jurisdictional claims in published maps and institutional affiliations.